Aerosol and Air Quality Research, 18: 2195–2206, 2018

ISSN: 1680-8584 print / 2071-1409 online
doi: 10.4209/aaqr.2017.11.0474

Characteristics of Classified Aerosol Types in South Korea during the MAPS-Seoul Campaign

Seoyoung Lee[1], Jaemin Hong[1], Yeseul Cho[1], Myungje Choi[1], Jhoon Kim[1,2], Sang Seo Park[3], Joon-Young Ahn[4], Sang-Kyun Kim[4], Kyung-Jung Moon[4], Thomas F. Eck[5], Brent N. Holben[5], Ja-Ho Koo[1*]

[1] *Department of Atmospheric Sciences, Yonsei University, Seoul 03722, Korea*
[2] *Harvard Smithsonian Center for Astrophysics, Cambridge, MA 02138, USA*
[3] *School of Earth and Environmental Sciences, Seoul National University, Seoul 08826, Korea*
[4] *National Institute of Environmental Research, Incheon 22689, Korea*
[5] *NASA Goddard Space Flight Center, Greenbelt, MD 20771, USA*

ABSTRACT

During the Megacity Air Pollution Studies-Seoul (MAPS-Seoul) campaign from May to June 2015, aerosol optical properties in Korea were obtained based on the AERONET sunphotometer measurement at five sites (Anmyon, Gangneung_WNU, Gosan_SNU, Hankuk_UFS, and Yonsei_University). Using this dataset, we examine regional aerosol types by applying a number of known aerosol classification methods. We thoroughly utilize five different methods to categorize the regional aerosol types and evaluate the results from each method by inter-comparison. The differences and similarities among the results are also discussed, contingent upon the usage of AERONET inversion products, such as the single scattering albedo. Despite several small differences, all five methods suggest the same general features in terms of the regionally dominant aerosol type: Fine-mode aerosols with highly absorbing radiative properties dominate at Hankuk_UFS and Yonsei_University; non-absorbing fine-mode particles form a large portion of the aerosol at Gosan_SNU; and coarse-mode particles cause some effects at Anmyon. The analysis of 3-day back-trajectories is also performed to determine the relationship between classified types at each site and the regional transport pattern. In particular, the spatiotemporally short-scale transport appears to have a large influence on the local aerosol properties. As a result, we find that the domestic emission in Korea significantly contributes to the high dominance of radiation-absorbing aerosols in the Seoul metropolitan area and the air-mass transport from China largely affects the western coastal sites, such as Anmyon and Gosan_SNU.

Keywords: Aerosol type classification; Optical property; AERONET; MAPS.

INTRODUCTION

Investigation of the regional radiative forcing is the essential step to figure out the climate change (Ramanathan and Carmichael, 2008; Shindell and Faluvegi, 2009). To determine the radiative forcing budget, how much solar radiation can be absorbed or scattered by regional aerosols should be inspected. Therefore, the type classification of airborne aerosols is the necessary process, which suggests the important information about the extent of radiative absorbing and scattering (Higurashi and Nakajima, 2002). Also, the accurate type classification is required to improve the quality of retrieval algorithm for aerosol products from the satellite measurement (Torres *et al.*, 2013; Sayer *et al.*, 2014). For these objectives, the aerosol type classification has been performed much, generally using aerosol optical properties obtained from the sunphotometer or skyradiometer measurements installed at some global ground-based networks such as the Aerosol Robotic Network (AERONET) (e.g., Holben *et al.*, 1998) and Skyradiometer Network (SKYNET) (e.g., Boi *et al.*, 1999).

The main idea for the aerosol type classification is to categorize aerosol properties into several groups based on the radiative absorptivity and size information of aerosols. The particle size is usually decided using fine-mode fraction (FMF), or Ångström exponent (AE) known to be positively correlated with the FMF (e.g., Eck *et al.*, 2008). The extent of radiative absorbing/scattering is mostly

* Corresponding author.
Tel.: 82-2-2123-2574; Fax: 82-2-365-5163
E-mail address: zach45@yonsei.ac.kr

decided based on the single scattering albedo (SSA). Thus, the combination of SSA and size information is the basic structure of type classification methods. For example, AERONET SSA and FMF (e.g., Lee *et al.*, 2010) or SSA and AE (e.g., Mielonen *et al.*, 2009) were directly compared to classify the black carbon, dust, non-absorbing, and mixture type of aerosols. The most popular method is to compare the absorbing and extinction AE, which are calculated using SSA and aerosol optical depth (AOD) values at multiple channels. There are many researches to apply this method (e.g., Russell *et al.*, 2010; Giles *et al.*, 2012; Mishra *et al.*, 2014; Alam *et al.*, 2016) for the separation of dust, biomass burning, and urban/industrial aerosols. Sometimes, only the wavelength dependence of SSA can be surveyed to distinguish aerosol types (e.g., Dubovik *et al.*, 2002; Russell *et al.*, 2010; Ali *et al.*, 2014; Li *et al.*, 2015).

While above mentioned researches are useful to have the information of regional aerosol types, there is a limitation about the number of available data because of the difficulty to retrieve SSA (Dubovik *et al.*, 2000a). Therefore, several previous studies have tried the aerosol type classification only based on simple aerosol optical properties such as AOD. The wavelength dependence of AOD has been mostly explored to pursue this goal. It has been known that the curvature shape of AOD spectral variation seems associated with not only the particle size (e.g., Eck *et al.*, 1999; Kaskaoutis and Kambezidis, 2006; Kumar *et al.*, 2014), but also the particle absorptivity (Koo *et al.*, 2016). Using this feature, several studies started to examine the characteristics of AOD spectral pattern at different wavelengths (i.e., AE from different wavelength pairs) in terms of the change of aerosol types (e.g., Schuster *et al.*, 2006; Gobbi *et al.*, 2007; Yoon *et al.*, 2012; Kolhe *et al.*, 2016). The ratio of AOD between different wavelengths can also be used for a type detection (Chen *et al.*, 2016). Comparison between AOD and AE is another approach frequently applied (Kumar *et al.*, 2014; Verma *et al.*, 2015; Yu *et al.*, 2015), but the criteria to distinguish aerosol types look much varied according to the region of research target.

At this present moment, it is hard to select the one best method for the type classification of regional aerosols because all methods were designed based on their own reasonable theoretical or empirical clues, supported by meaningful validation results. Therefore, there is an interest to see how consistent or different these different methods are for same place and time period. To pursue this objective, we apply various methods to the classification of aerosol type in the Korean Peninsula using the AERONET observations during the Megacity Air Pollution Studies-Seoul (MAPS-Seoul) campaign, conducted from 18 May to 14 June 2015. Usually in this season, both local emission and air-mass transport influence can be found simultaneously (Koo, 2008), which is the appropriate condition for the analysis of regional aerosol properties. We apply various kinds of classification methods for the same region and period and compare obtained results with each other. Comparisons of multiple results will be useful to evaluate the performance of each classification method, resulted in better understanding of regional properties of dominant aerosol types. In particular, how classified types from methods without using SSA relate to those from methods based SSA information will be focused. The pattern of regional air-mass transport will be also discussed to explain the obtained classified types.

SITE AND DATA DESCRIPTION

Site information

During the MAPS-Seoul campaign, aerosol optical properties have been observed using the AERONET sunphotometers (https://aeronet.gsfc.nasa.gov/) installed in the Korean Peninsula. In this study, we use measurement data at five AERONET stations (Fig. 1): Anmyon (36.54°N, 126.33°E), Gangneung_WNU (37.77°N, 128.87°E), Gosan_SNU (33.29°N, 126.16°E), Hankuk_UFS (37.34°N, 127.27°E), and Yonsei University (37.56°N, 126.94°E). Anmyon is the small island located near the western coast of the Korean Peninsula. This site is basically regarded as the rural characteristic but often affected by the strong influence of air pollutant transport from China (Chun *et al.*, 2001). Gangneung_WNU site is located in the small urban area in the eastern coast of the Korean Peninsula, and relatively far from the air pollutant transport from the China. Gosan_SNU site is located in the southwest of Jeju Island on the Southern Sea of South Korea, showing the weak air pollution locally. However, Gosan_SNU site also shows high aerosol concentrations sometimes when the strong transboundary transport occurs from China (Kim *et al.*, 2012; Shang *et al.*, 2018), similar to other stations. Hankuk_UFS is the sub-urban area near the Seoul Metropolitan Area (SMA), probably affected by the short-range air-mass transport from the SMA. Yonsei_University is located in the middle of Seoul city, one of the large megacities in the world. Thus, the high local aerosol emission is expected different from other rural sites. Owing to its location, this site also lies under the influence of westerly from China.

Data Description

At each station, the AERONET sunphotometer measures radiance from the ultraviolet to near-infrared channels. Various kinds of aerosol optical properties are computed using these radiance values with retrieval algorithm. These properties are provided at the seven representative channels: 340, 380, 440, 500, 675, 870, and 1020 nm. For the various aerosol type classifications in this study (more details in the next section, Methods), we mainly use AOD, SSA, extinction Ångström exponent (EAE), absorption Ångström exponent (AAE), and FMF values at these multiple channels. AOD typically shows the extent of atmospheric turbidity due to the aerosol loading. SSA indicates how much solar radiation is absorbed or scattered by regional airborne aerosols. EAE represents the spectral dependence of AOD and it provides size information of aerosols. Generally, a high value of EAE indicates a small particle and small value of EAE indicates large particle, but it varies with the selection of wavelength pair (Eck *et al.*, 1999; Reid *et al.*, 1999). Similar to EAE, AAE indicates

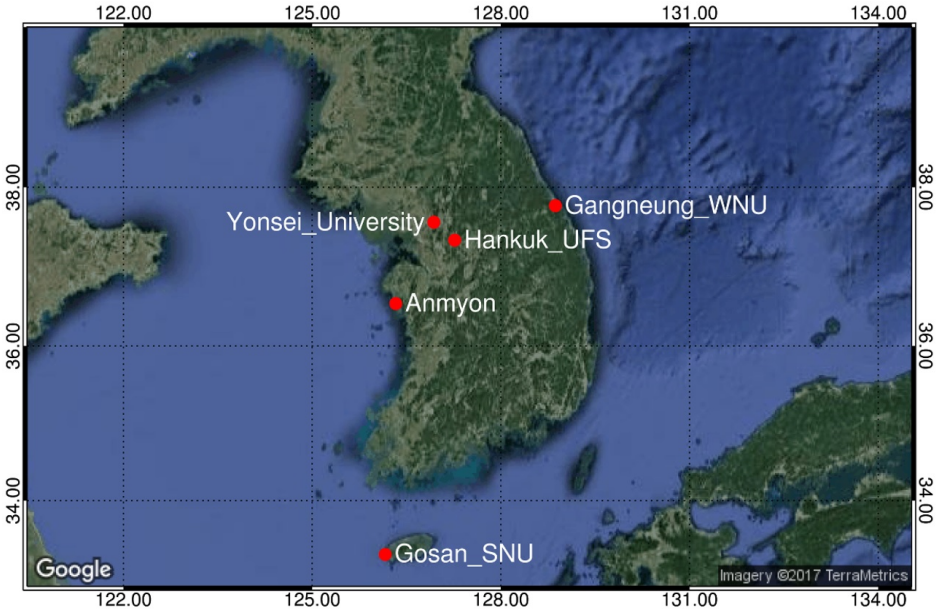

Fig. 1. The location of AERONET sites used in this study for the aerosol type classification during the MAPS-Seoul campaign.

spectral dependence of absorption AOD and depends upon aerosol composition (Bergstrom *et al.*, 2007; Russell *et al.*, 2010). The theoretical value of AAE is 1 for black carbon, and can be greater than 2 for dust type aerosols (Bergstrom *et al.*, 2002; Bergstrom *et al.*, 2007). Finally, FMF defined as the ratio of the fine-mode AOD to the total AOD is also used to represent aerosol size. In this study, FMF at 550 nm is obtained by considering EAE and fine-mode AOD at AERONET wavelengths.

The AOD and AE are obtained from attenuated direct-sun measurement (Holben *et al.*, 1998). FMF is calculated from direct-sun measurement with the spectral deconvolution algorithm (O'Neill *et al.*, 2003) or almucantar measurement of scattered radiance in the whole sky with the statistically optimized inversion algorithm (Dubovik *et al.*, 2000b). SSA is another product obtained from the inversion algorithm using almucantar measurements, only available from 440, 675, 870, and 1020 nm and implemented when solar zenith angle is greater than 50°. These inversion products can be processed when the low retrieval uncertainty is guaranteed. For example, SSA values are significantly taken into account just for the case showing that AOD is higher than 0.4 because of usual large uncertainty of SSA in the pristine area (Dubovik *et al.*, 2000b).

In accordance with the data quality, AERONET has the three levels of dataset: Level 1.0, 1.5, and 2.0. Level 1.0 data are all unscreened values, and Level 1.5 data can be prepared after cloud screening processes (Smirnov *et al.*, 2000). Level 2.0 data provide the best quality assured information with additional quality control and quality assurance process with the detail information from the instrumental calibration. For all methods of aerosol type classification treated in this study, we utilize "all-points" level 2.0 dataset of the AERONET Version 2 product to avoid the misleading interpretation for the result analysis.

Related to the analysis of AERONET measurements, we also use the back-trajectory information to figure out the pattern of regional air-mass transport. For the back-trajectory calculation, we use the Hybrid Single Particle Lagrangian Integrated Trajectory Model version 4 (HYSPLIT4) provided from the National Oceanic and Atmospheric Administration (Stein *et al.*, 2015). For five stations mentioned above, 3-day back trajectories are calculated for every hour during the MAPS-Seoul campaign, supposing the arrival height at 500 m. In this process, the Global Data Assimilation System (GDAS) with 1° by 1° resolution is used for the meteorological field information.

METHODS

Among various classification algorithms, which have been inspected so far, we try to apply total five classification methods based on AERONET measurements during the MAPS-Seoul campaign. Each method has own characteristics, thus inter-comparison of aerosol types obtained from these different methods will be useful to have a better idea for the dominant aerosol properties in late spring and early summer of South Korea. Here we describe the details of each method shortly.

The first method (M1) is the way to use single channel SSA and FMF. Lee *et al.* (2010) utilized SSA at 440 nm and FMF at 550 nm to discriminate four different kinds of aerosols: dust, mixture, non-absorbing, and black carbon aerosols. In this method, coarse-mode particles (FMF < 0.4) are mostly decided as dust particle, and middle-size particles (FMF between 0.4 and 0.6) are decided as mixture. For fine-mode particles (FMF > 0.6), aerosols having high radiative scattering (SSA > 0.95) are decided as non-absorbing aerosols, and aerosols having high radiative absorbing (SSA ≤ 0.95) are decided as black carbon (BC).

Black carbon types are also separated into three ranges according to the extent of SSA: slightly-, moderately-, and highly- absorbing BC. Since SSA values from AERONET level 2 data are only valid when AOD is higher than 0.4 due to the uncertainty of inversion calculation (Dubovik *et al.*, 2000a, Holben *et al.*, 2006), non-absorbing coarse-mode aerosols are not clearly categorized in this method.

The second method (M2) is designed based on the comparison between EAE and AAE. This method intends to inspect the spectral variation of AOD for absorption and scattering parts separately. Using the AOD and SSA values, absorption AOD (AAOD) is easily estimated at all channels. And then AAE is calculated based on the spectral dependence of AAOD (Russell *et al.*, 2010; Giles *et al.*, 2012). For the EAE, generally AERONET AE values at 440–870 nm are directly utilized. Many previous studies have tried to classify the aerosol type using these AAE and EAE values, but they have supposed their own criteria, largely varied each other. Particularly threshold values of AAE for the aerosol type separation show a quite large difference according to the target region (Mishra and Shibata, 2012). Here, we refer to the classification process in Giles *et al.* (2012), which tried their best to generate the globally consistent categories. Regardless of difficulty to designate the exact threshold among particle types, dust type (AAE: ~1.5–2.3, EAE: ~0.2–0.3) is rather well separated from urban/industrial and biomass burning aerosol type (AAE: ~1.0–1.5, EAE: ~1.5–2.0). Biomass burning type shows a little higher EAE than urban/industrial type, implying the smaller particle size. The range of AAE and EAE for mixture aerosols is found between dust and urban/industrial type, as shown in Giles *et al.* (2012).

The third method (M3) is based on the wavelength dependence of single scattering albedo. Li *et al.* (2015) showed the spectral dependence of SSA can have sensitivity for the aerosol type classification. These SSA spectral patterns are primarily attributed to the high radiative absorption by dust at the shorter wavelength, and by black carbon at the longer wavelength. As a result, dust particle reveals the lower SSA at the shorter wavelength but higher SSA at the longer wavelength. In contrast, urban/industrial and biomass burning aerosol types show the higher SSA at the shorter wavelength and lower SSA at the longer wavelength. With a similar spectral pattern, the urban/industrial aerosol type has higher SSA values than the biomass burning type for all visible and near-IR channels. Mixture type has a peculiar spectral curvature of SSA: Maximum SSA appears at 675 nm (Li *et al.*, 2015).

From M1 to M3, all classification methods use the SSA value, which is generated from the AERONET inversion algorithm. As mentioned above the number of SSA product from the inversion process is not enough for the analysis usually (Table 1). Owing to this limitation, we also consider other type classification methods without using SSA. This different idea has started because some previous studies found that the wavelength difference of AOD has the meaningful sensitivity to the aerosol types (e.g., Yoon *et al.*, 2012). Thus, we will compare new classification results with those of M1 to M3 to figure out how much different the classified aerosol type is in terms of whether dealing with SSA or not.

The fourth method (M4) only examines the AOD values at different wavelengths. Chen *et al.* (2016) categorized six different aerosol types (maritime, desert dust, continental, sub-continental, urban industry, and biomass burning type) using AOD at 440 nm and AOD ratio between 440 and 1020 nm, called aerosol relative optical depth (AROD). Thresholds for each aerosol type are designated based on variations of AODs and ARODs with considering fluctuation of aerosol concentration and imaginary part of refractive index for six aerosol types: maritime (AOD $\leq$ 0.15, AROD $\geq$ 0.31) , continental (0.15 $\leq$ AOD $\leq$ 0.5, AROD $\leq$ 0.81 or AOD $\leq$ 0.15, AROD $\leq$ 0.31), desert dust (AOD $\geq$ 0.15, AROD $\geq$ 0.81), sub-continental (AOD $\geq$ 0.5, 0.39 $\leq$ AROD $\leq$ 0.81), urban industry (AOD $\geq$ 0.5, 0.25 $\leq$ AROD $\leq$ 0.39), and biomass burning aerosols (AOD $\geq$ 0.5, AROD $\leq$ 0.25). In general, maritime and continental type can be distinguished for the lower 440 nm AOD case (AOD < 0.15) because it is known that the AOD at 440 nm of maritime aerosol usually does not exceed 0.15 (Dubovik *et al.*, 2002). Dust, sub-continental, urban/industrial, and biomass burning type can be separated based on the AROD for the high AOD case. The basic idea of this method is devised based on the fact that different aerosol compositions have different AROD patterns (Yuan *et al.*, 2014), and therefore resulted in the easier analysis with direct measurement of aerosol optical properties from AERONET network.

The fifth method (M5) is applied for the type classification

Table 1. The statistics for AERONET inversion and direct sun data products at each site during the MAPS-Seoul campaign.

		Anmyon	Gangneung_ WNU	Gosan_SNU	Hankuk _UFS	Yonsei _University
Inversion	Number of data	7	12	3	10	24
	SSA at 440 nm	0.946	0.953	0.987	0.912	0.920
	FMF at 550 nm	0.788	0.828	0.980	0.888	0.887
	AAE at 440–870 nm	1.552	1.382	1.200	1.296	1.595
	EAE at 440–870 nm	1.170	1.284	1.199	1.379	1.331
Direct Sun	Number of data	505	759	1236	289	663
	AOD at 440 nm	0.284	0.290	0.261	0.433	0.393
	AOD at 1020 nm	0.097	0.087	0.082	0.139	0.124
	AAE at 480–500 nm	1.337	1.396	1.479	1.266	1.335
	AAE at 500–870 nm	1.299	1.362	1.511	1.403	1.344

using the wavelength dependence of AE, i.e., spectral curvature pattern of AOD in a logarithmic scale. Eck *et al.* (1999) found that there is a contrast of AOD spectral pattern between fine- and coarse-mode dominant condition. In other words, AE values reveal large differences according to the selected wavelength pairs. Koo *et al.* (2016) made a progress about this feature more. They investigated the pattern of AE ratio (AER) between shorter (380–500 nm) and longer (500–870 nm) wavelength pairs, related to the spectral curvature of AOD: AER < 1.0 for the absorbing coarse-mode dominant case, AER close to 1.0 for the scattering fine-mode dominant case, and AER > 2.0 for the existence of fine-mode particles having the UV absorption. As a result, AER change also seems associated with the aerosol type variation. This method can be another approach for the aerosol type classification without utilizing AERONET inversion product such as SSA.

RESULTS AND DISCUSSION

Characteristics of all five classification methods described in Methods section are summarized in Table 2. Based on these methods, now we assort regional aerosol types at five AERONET stations during the MAPS-Seoul campaign. We try to interpret results from each method, and compare them to see if there is a large similarity or difference. After that, we investigate the pattern of back-trajectories to understand how the regional aerosol types relate to the origin of regional air masses.

Classified Aerosol Type at Each Site

Fig. 2 illustrates classified results from M1 for five stations. In general, BC type aerosols are much detected. Only Gosan_SNU station shows the dominance of non-absorbing aerosols. This difference may come from the regional characteristic. Since Gosan_SNU site is located far from the land and surrounded by the ocean, small size particles from urban and industrial area are not much expected. Considering that the air-mass transport from the west usually affects the local air quality at Gosan and Jeju Island (Kim *et al.*, 2012; Shang *et al.*, 2018), fine-mode particle having high radiative scattering (e.g., some kinds of organic aerosols) can be dominantly transported into Gosan_SNU site during the period of the MAPS-Seoul campaign. Other sites usually show the dominance of BC type aerosols. Patterns at Anmyon, Gangneung_WNU, Hankuk_UFS, and Yonsei_University reveal the higher radiative absorptivity (depicted by some portion of moderate absorption in Fig. 1), which looks the contribution of local pollutant emission from the urban or sub-urban sites. Mixture type does not seem general in this method; only Yonsei_University site shows the ~10% mixture type.

For same sites, we now apply M2 using AAE and EAE and compare results (Fig. 3). In general, mean EAE is the

Table 2. Brief description of aerosol type classification methods used in this study.

Method	Main reference	Used parameters
M1	Lee *et al.* (2010)	SSA at 440 nm and FMF at 550 nm
M2	Giles *et al.* (2012)	Absorption and Extinction Ångström exponents at 440–870 nm
M3	Russell *et al.* (2010), Li *et al.* (2015)	SSA at 440, 675, 870, and 1020 nm
M4	Chen *et al.* (2016)	AOD at 440 nm and AOD ratio between 440 and 1020 nm
M5	Eck *et al.* (1999), Koo *et al.* (2016)	Ångström exponent at short and long wavelength pairs

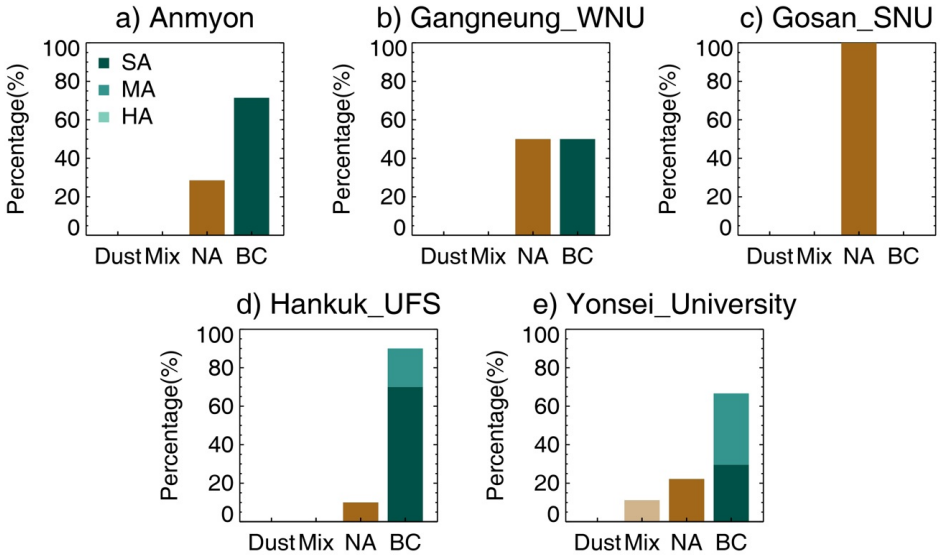

Fig. 2. Classified aerosol types using method 1 (M1) during the MAPS-Seoul campaign at (a) Anmyon, (b) Gangneung_WNU, (c) Gosan_SNU, (d) Hankuk_UFS, and (e) Yonsei_University sites. SA, MA, and HA imply the slightly, moderately, and highly radiative absorbing due to the BC type.

smallest at Anmyon and highest at Hankuk_UFS and Yonsei_University. AAE are ~1.0 to 1.5 on average but reveal broader ranges, Anmyon and Yonsei_University in particular. Based on the cluster analysis in Giles *et al.* (2012), aerosol type results at all five sites look close to the mixture type and partially urban/industrial type can be found at the Hankuk_UFS and Yonsei_University sites. In contrast, some patterns at Anmyon are relatively close to the dust type (small EAE and large AAE). Considering that slightly absorbing BC type is found as the most dominant type by M1 (Fig. 2), some part of mixture decided by M2 criteria may still relate to the dominance of absorbing particles. Since many previous researches have utilized different threshold values for classifying the regional aerosol type based on M2 (Mishra and Shibata, 2012), M2 cannot effectively separate aerosol types. Namely, the classification method using AAE and EAE may have a difficulty to capture the subtle variation in a local scale although that is still useful for the general type detection. In sum, we presume that the meaning of mixed category from M2 looks to present that there can be various kinds of aerosols simultaneously in the Korean Peninsula during the MAPS-Seoul campaign.

M3 is next applied for the type categorization, using the wavelength dependence of SSA (Fig. 4). Despite small differences, it seems that all five sites have their own properties. While Gangneung_WNU and Gosan_SNU sites depict almost flat spectral dependence of SSA, there is a subtle difference: SSA increase in longer wavelengths at Gangneung_WNU, but SSA decrease at Gosan_SNU. Considering that generally lower SSA in shorter wavelengths implies the dust-type dominance and higher SSA in shorter wavelengths relates to the urban/industrial or biomass burning types (Russell *et al.*, 2010; Li *et al.*, 2015), probably Gangneung_WNU site is a little affected by transported dust particles. But Gosan_SNU site showing the highest SSA is affected by fine-mode non-absorbing particles when the regional atmosphere is polluted. But again, this interpretation may have little meaning because the SSA spectral variation is too small. Hankuk_UFS site shows rather clear SSA decrease as longer wavelengths, implying that the urban/industrial aerosols are dominant, consistent with the finding from M1 and M2 analysis. Yonsei_University site reveals a little different pattern: maximum peak at 675 nm meaning the mixture type as stated in Li *et al.* (2015). Considering the large influence of Asian dust particles and Chinese pollutants during springtime at Seoul (Jung *et al.*, 2010; Jeong *et al.*, 2011), Yonsei_University can have atmospheric conditions composed of transported natural dust and local urban/industrial pollutants. This highest SSA at 675 nm may explain why M1 only shows the portion of mixture type at the Yonsei_University site. At Anmyon, low SSA at 440 nm and high SSA at infrared channels looks to indicate the dust type. But the meaning of M3 result at Anmyon is not clear because the dust type at Anmyon was not found in M1 and M2 method.

From now on, we examine results from methods without using SSA. Fig. 5 shows the portion of six categories determined from M4 analysis, which utilizes AOD at 440 nm and AROD between 440 and 1020 nm. Overall, continental type aerosols look the most dominant for all five sites. Also, we can find the partial existence of maritime aerosols for the sites located in the coastal region (Anmyon, Gangneung_WNU, and Gosan_SNU). M4 can determine maritime and continental aerosol types when the AOD is lower (Chen *et al.*, 2016), which is not found in M1, M2, and M3. Thus, M4 results indicate that local dominant aerosol type can be much different in accordance with the extent of air pollution. In other words, M1, M2, and M3 analysis only let us know which aerosol type can mostly contribute to the increase of local aerosol amount. But if you would

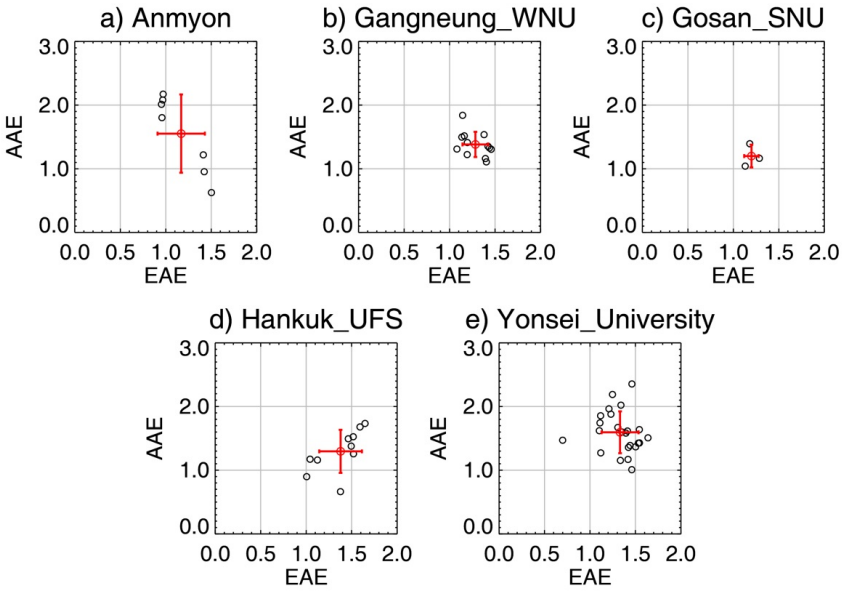

Fig. 3. Relationships between AAE and EAE based on method 2 (M2) during the MAPS-Seoul campaign at (a) Anmyon, (b) Gangneung_WNU, (c) Gosan_SNU, (d) Hankuk_UFS, and (e) Yonsei_University sites. Vertical and Horizontal bars indicate the 1-σ standard deviation of AAE and EAE values at each site.

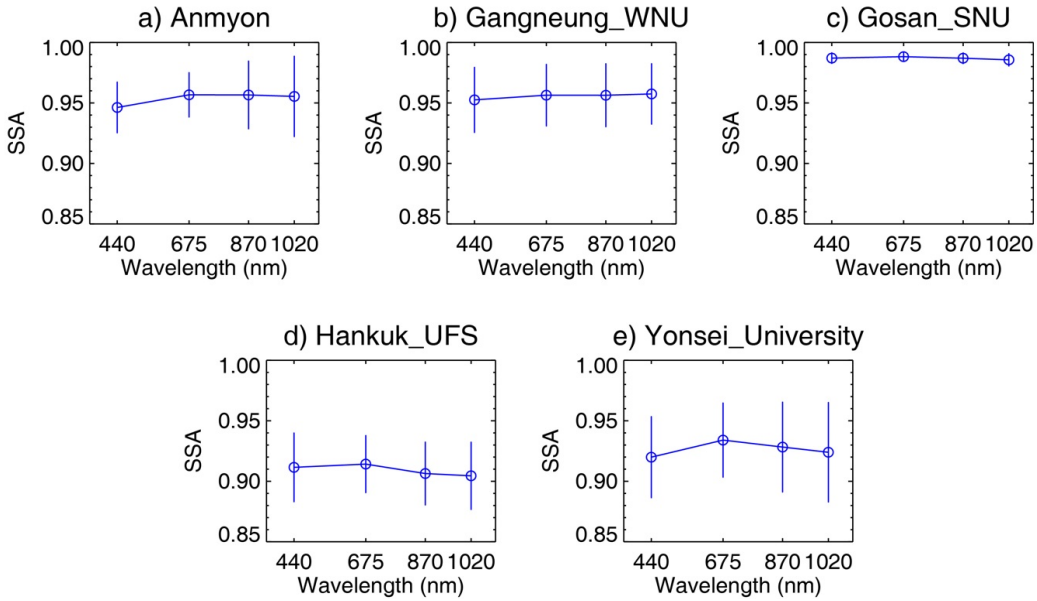

Fig. 4. Spectral variation of SSA based on method 3 (M3) during the MAPS-Seoul campaign at (a) Anmyon, (b) Gangneung_WNU, (c) Gosan_SNU, (d) Hankuk_UFS, and (e) Yonsei_University sites. Vertical bar indicates the 1-σ standard deviation of all SSAs values measured at each channel.

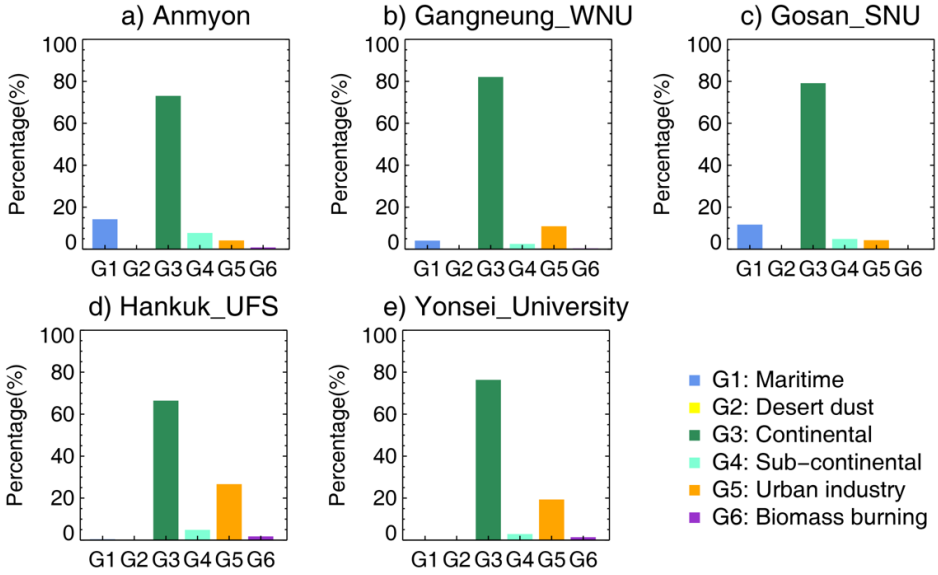

Fig. 5. Classified aerosol types using method 4 (M4) during the MAPS-Seoul campaign at (a) Anmyon, (b) Gangneung_WNU, (c) Gosan_SNU, (d) Hankuk_UFS, and (e) Yonsei_University sites.

find the dominant aerosol type of regional background atmosphere and its frequency, interpretation based on results from M1, M2, and M3 is not proper. This reveals the necessity to perform the inter-comparison of various classification methods. Except continental and maritime aerosols, the urban industry aerosol seems the next dominant particle. Fig. 5 indicates that the portion of urban industry aerosol types shows the highest portion at Hankuk_UFS, but the lowest at Anmyon and Gosan_SNU, illustrating that M4 has the possibility to distinguish the aerosol type between the urban and rural area. However, M4 fails to find a difference between Anmyon and Gosan_SNU, detected in previous methods. This feature shows the limitation for separating between the radiative absorption and scattering in the rural area, attributed to non-usage of the information such as SSA.

At last, we examine results from M5, which is based on the spectral curvature of AOD. Following the approach in Koo *et al.* (2016), AER values are calculated to divide longer AE (AE at 500–870 nm) by shorter AE (AE at 380–500 nm). The distribution of AER values at five sites are illustrated as Fig. 6. Patterns at Gangneung_WNU and Yonsei_University are quite similar each other: high portion of AER values between 0.95 and 1.05, meaning the

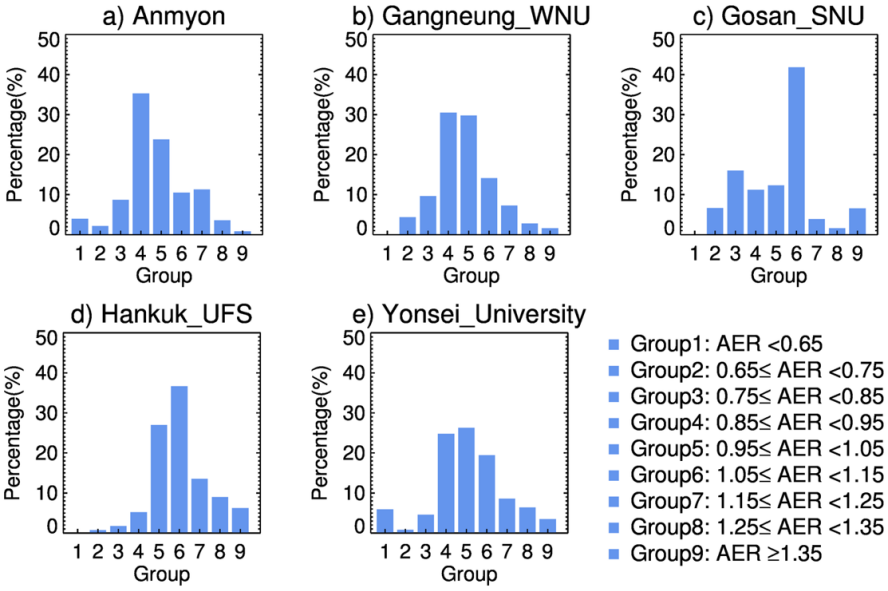

Fig. 6. Percentage variations of AER based method 5 (M5) during the MAPS-Seoul campaign at (a) Anmyon, (b) Gangneung_WNU, (c) Gosan_SNU, (d) Hankuk_UFS, and (e) Yonsei_University sites.

almost linear relationship between AODs and wavelengths in a logarithmic scale. It seems that these sites are not purely described as fine- or coarse-mode dominance, but probably composed of fine- and coarse-mode mixtures (Eck *et al.*, 1999). Anmyon also has the similar pattern in spite of somewhat higher portion of AER values in 0.85–0.95 range, showing the relatively larger contribution by coarse-mode aerosols. The Hankuk_UFS site also reveals the high portion of AER values near ~1.0 but a little skewed to the AER > 1.0, different from the Gangneung_WNU, and Yonsei_University sites, implying the relatively higher contribution of fine-mode aerosols in this site. Gosan_SNU shows the discriminative portion of AER values in 1.05–1.15 range, indicating the large dominance of fine-mode aerosols relatively. Different from M4, M5 can find the difference of dominant aerosol type between Anmyon and Gosan_SNU.

We examined and compared aerosol classification results from five methods. In brief, most of sites have mixed conditions of aerosol types except Gosan_SNU, located in the Jeju Island. The aerosol type at Gosan_SNU looks rather distinguishing, showing the large dominance of non-absorbing particles in the fine-mode range. Hankuk_UFS, and Yonsei_University sites similarly show the influence of urban/industrial types. Among them, Hankuk_UFS looks to have the largest dominance of urban type fine-mode aerosols having high radiative absorbing properties, but Yonsei_University shows the higher dominance of mixture type of aerosols relatively. Despite some portion of radiative absorbing particles, results indicate that Anmyon seems affected by a relatively larger influence of coarse-mode aerosols based on finding of M2, M3 and M5.

Back-trajectory Analysis

Here we conduct a back-trajectory analysis to more investigate the difference or similarity of regional aerosol types in terms of the relationship to emission sources. During the MAPS-Seoul campaign, we try to pursue the origin of air-masses arrived at each site using 3-day back-trajectories calculated every hour. Potential source regions are separated into total six categories from R1 to R6 (Fig. 7). R1 implies the Korean domestic contribution, and R2 means the North Chinese source of long-range transport. R3 and R4 indicate the contribution of eastern Chinese air masses: Beijing and the Shandong Peninsula are located in R3, but the southern Chinese area belongs to the R4. R5 and R6 covers the southern and east oceanic area, respectively.

We first put all 3-day back-trajectories at each site on the map and see which region mainly play a role as the influential origin of the transported air masses (Fig. 7). Generally, most sites have a large portion of air-masses come from the northern and eastern China except Gosan_SNU. Gosan_SNU site is more affected by the air-mass transport from the southern oceanic area, which is R5 region. Anmyon also has some transported air masses from R5 region, but shows more back-trajectories from China, which are R2, R3, and R4. Gangneung_WNU, Hankuk_UFS, and Yonsei_University reveal the similar pattern of back-trajectories. However, Hankuk_UFS and Yonsei_University depict relatively shorter back-trajectories (i.e., slower air-mass transport) while back-trajectories at Gangneung_WNU more indicate the pattern of long-range transport from northern China.

For better examining the regional transport contribution, we compare the direction of back-trajectories for the period of 1, 2, and 3 days before the arrival. First, each 3-day back-trajectory is split into the three periods: 1–24 hours (i.e., 0–1 day), 25–48 hours (i.e., 1–2 days), 49–72 hours (i.e., 2–3 days) before arrival. Then the region (R1 to R6) where a back-trajectory mostly passes over are counted for each period. After repeating this process for the whole MAPS-Seoul campaign, then a pie chart is prepared to depict how frequent each region (R1–R6) is counted for three periods.

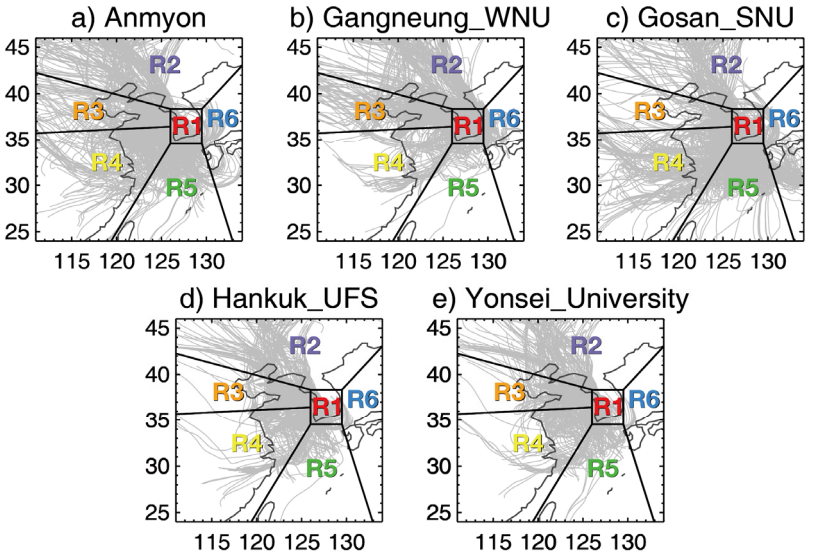

Fig. 7. All 3-day back-trajectories for every hour during the MAPS-Seoul campaign at (a) Anmyon, (b) Gangneung_WNU, (c) Gosan_SNU, (d) Hankuk_UFS, and (e) Yonsei_University sites. Six regions (R1, R2, R3, R4, R5, and R6) are separated to examine where transported air-masses come from.

This process is applied to all five sites. All results are finally shown as Fig. 8.

Fig. 8 illustrates that there are three back-trajectory patterns separated in general: Anmyon/Gosan_SNU/Gangneung_WNU, Hankuk_UFS, and Yonsei_University. Considering the back-trajectory pattern at 1–24 hours before arrival, R3 (eastern China) shows the largest contribution to Anmyon, but R5 (southern oceanic area of Korean Peninsula) reveals the largest contribution to Gosan_SNU. Gangneung_WNU, Hankuk_UFS, and Yonsei_University have the highest influence from the air-masses from R1, indicating the large domestic effect. These three rough groups are rather well matched to the discriminated pattern of regional aerosol types found using five classification methods: the peculiar dominance of non-absorbing fine-mode aerosols at Gosan_SNU, the dominance of high radiative absorbing particles at Gangneung_WNU, Hankuk_UFS, and Yonsei_University, and relatively high influence of coarse-mode particles at Anmyon. This looks a clue that the regional aerosol properties can be strongly associated with the pattern of air-mass transport.

Then we will more discuss for how the location of back-trajectories relates to the dominant aerosol types at each site. For Anmyon, most back-trajectories stay in R3 and R4 at 1–24 hours before arrival, indicating that the large influence of air pollution transport emitted from eastern China. In contrast, most back-trajectories at 1–24 hours before arrival to Gangneung_WNU, Hankuk_UFS, and Yonsei_University stay in R1. However, this contrast does not appear when we compare earlier back-trajectories. In other words, almost ~75% of back-trajectories passes over the R2, R3, or R4 regions (i.e., Chinese area) for 25–72 hours before arrival at all sites except Gosan_SNU. Even ~60% of back-trajectories are found over R2, R3, and R4 for 25–72 hours before arrival at Gosan_SNU. This finding reveals that the transported air masses from China has some impacts to all sites in the Korean Peninsula consistently, but the pattern of short-range transport seems more associated with the regional difference of classified aerosol types.

Focusing on the pattern of first 24-hour back-trajectories, Gangneung_WNU, Hankuk_UFS, and Yonsei_University are most frequently affected by the air-mass from R1. Considering classified results at these sites, Korean domestic emissions look to influence largely on the dominance of high radiative absorbing aerosols. At Anmyon, the largest short-range transport of air masses occurs over R3, meaning that the air pollutant emitted in Beijing-Tianjin-Hebei area or the Shandong Peninsula can be associated with the aerosol properties at Anmyon. But we need to remember that M4 results actually show the highest portion of maritime and sub-urban type (Fig. 5) and M5 results show the dominance of coarse-mode particles (Fig. 6) in this site. Perhaps, sea salt aerosols in the Yellow Sea (between eastern China and the Korean Peninsula) is transported into Anmyon by westerlies in this time. Actually, this idea better explains the classified aerosol type at Anmyon. Meanwhile, Gosan_SNU shows ~55% of the first 24-hour back-trajectories passing over R5, showing that the southern oceanic area looks the origin of non-absorbing aerosols, the dominant type in this site.

In conclusion, the analysis of back-trajectories is useful to understand the regional property of aerosol types better. An interesting point is that the type separation looks associated with not only the feature of air-mass transport, but also the latitude of site location (Gosan_SNU/Anmyon/other sites). Based on this finding, we can presume that the regional meteorological pattern in the Korean Peninsula may differ in accordance with the latitude, induce the different pattern of air-mass transport latitudinally, finally results in the regional difference of dominant aerosol types. More synthetic analysis will be required with connecting the synoptic meteorological pattern and regional aerosol types.

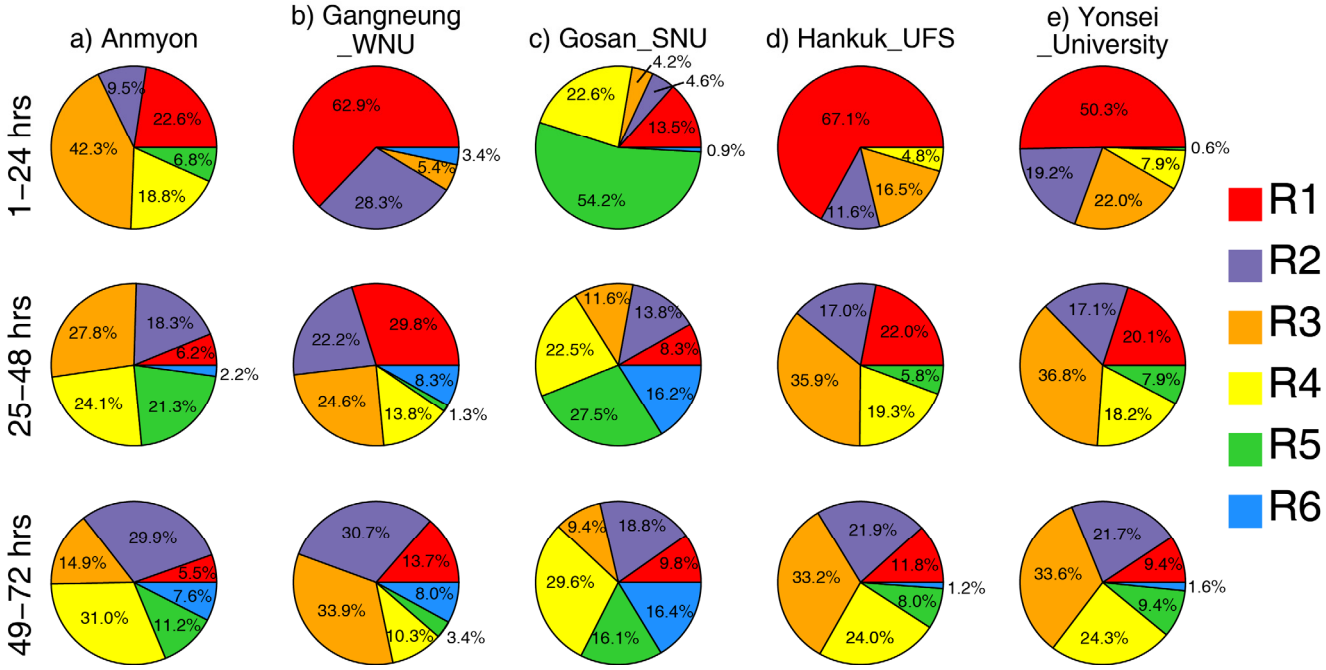

Fig. 8. Pie charts showing where back-trajectories (meaning transported air-masses) dominantly stay before arrival to (a) Anmyon, (b) Gangneung_WNU, (c) Gosan_SNU, (d) Hankuk_UFS, and (e) Yonsei_University sites, considering six separated regions: cases for 1 to 24 hours before arrival (top), cases for 25 to 48 hours before arrival (middle), and cases for 49 to 72 hours before arrival (bottom).

SUMMARY AND CONCLUSION

We investigated the regionally dominant aerosol types using the AERONET measurements from the MAPS-Seoul campaign at five sites located on the Korean Peninsula. We thoroughly utilized five different methods based on different combinations of aerosol optical properties obtained from AERONET products. Although each method can identify the dominant pattern in regional aerosol types, some differences exist among the results, which means that analysis based on a single classification method may be insufficient. Thus, an effort to take consistent findings into account for a better understanding of regional aerosol types is required. Using the five methods in this study, we can estimate some regional characteristics of our own: the high radiative absorptivity of the major portion of urban/industrial aerosols at Hankuk_UFS, the dominance of non-absorbing fine-mode particles at Gosan_SNU, the mix of fine- and coarse-mode aerosol types at Yonsei_University, some effects from coarse-mode particles at Anmyon, and so on.

We also examined the pattern of short-range back-trajectories at each site to identify which regions are potential sources of the dominant aerosol type. When the back-trajectories mostly remain over the Korean Peninsula before arrival, the regionally dominant type is classified as a high-radiation-absorbing aerosol, indicating the contribution of domestic emissions (for example, at Gangneung_WNU, Hankuk_UFS, and Yonsei_University). More air-mass transport from eastern China seems to induce the dominance of coarse-mode aerosols at Anmyon, probably due to the effect of sea salt emitted from the Yellow Sea. The dominance of non-absorbing aerosol types at Gosan_SNU appears to be associated with aerosols from southern China passing over the southern oceanic area, probably due to the aging process (Lee *et al.*, 2017). While our analyses in this study are reasonably well performed based on measurements from the MAPS-Seoul campaign, we still need to analyze other time periods to determine whether these findings will be consistent. Continuous works have finally given us an improved angle on classification based on the AERONET platform, and upgrading the satellite algorithm for classification (e.g., Kim *et al.*, 2007; Mok *et al.*, 2016) in the future will also be very useful.

ACKNOWLEDGMENTS

This subject was funded by Korea Ministry of Environment (MOE) as the Public Technology Program based on Environmental Policy (2017000160001). This research was also supported by the National Strategic Project-Fine Particle of the National Research Foundation of Korea (NRF) funded by the Ministry of Science and ICT (MSIT), the Ministry of Environment (ME), and the Ministry of Health and Welfare (MOHW) (NRF-2017M3D8A1092021). The authors gratefully acknowledge the NOAA Air Resources Laboratory (ARL) for the provision of the HYSPLIT transport and dispersion model and READY website (http://www.ready.noaa.gov) used in this publication. We also thank the AERONET principal investigators (Drs. Chulkyu Lee, Kyu-Tae Lee, Sang-Woo Kim, Young Sung Ghim, and Jhoon Kim) and their staff for establishing and maintaining the Anmyon,

Gangneung_WNU, Gosan_SNU, Hankuk_UFS and Yonsei_University sites used in this study.

REFERENCES

Alam, K., Shaheen, K., Blaschke, T., Chishtie, F., Khan, H.U. and Haq, B.S. (2016). Classification of aerosols in an urban environment on the basis of optical measurements. *Aerosol Air Qual. Res.* 16: 2535–2549.

Ali, M., Tariq, S., Mahmood, K., Daud, A., Batool, A. and Haq, Z. (2014). A study of aerosol properties over Lahore (Pakistan) by using AERONET data. *Asia-Pac. J. Atmos. Sci.* 50: 153–162.

Bergstrom, R.W., Pilewskie, P., Russell, P.B., Redemann, J., Bond, T.C., Quinn, P.K. and Sierau, B. (2007). Spectral absorption properties of atmospheric aerosols. *Atmos. Chem. Phys.* 7: 5937–5943.

Bergstrom, R.W., Russell, P.B. and Hignett, P. (2002). Wavelength dependence of the absorption of black carbon particles: Predictions and results from the TARFOX experiment and implications for the aerosol single scattering albedo. *J. Atmos. Sci.* 59: 567–577.

Boi, P., Tonna, G., Dalu, G., Nakajima, T., Olivieri, B., Pompei, A., Campanelli, M. and Rao, R. (1999). Calibration and data elaboration procedure for sky irradiance measurements. *Appl. Opt.* 38: 896–907.

Chen, Q.X., Yuan, Y., Shuai, Y. and Tan, H.P. (2016). Graphical aerosol classification method using aerosol relative optical depth. *Atmos. Environ.* 135: 84–91.

Chun, Y., Boo, K.O., Kim, J., Park, S.U. and Lee, M. (2001). Synopsis, transport, and physical characteristics of Asian dust in Korea. *J. Geophys. Res.* 106: 18461–18469.

Dubovik, O., Smirnov, A., Holben, B.N., King, M.D., Kaufman, Y.J., Eck, T.F. and Slutsker, I. (2000a). Accuracy assessment of aerosol optical properties retrieval from AERONET sun and sky radiance measurements. *J. Geophys. Res*. 105: 9791–9806.

Dubovik, O. and King, M.D. (2000b). A flexible inversion algorithm for retrieval of aerosol optical properties from Sun and sky radiance measurements. *J. Geophys. Res.* 105: 20673–20696.

Dubovik, O., Holben, B.N., Eck, T.F., Smirnov, A., Kaufman, Y.J., King, M.D., Tanré, D. and Slutsker, I. (2002). Variability of absorption and optical properties of key aerosol types observed in worldwide locations. *J. Atmos. Sci.* 59: 590–608.

Eck, T.F., Holben, B.N., Reid, J.S., Dubovik, O., Smirnov, A., O'Neill, N.T., Slutsker, I. and Kinne, S. (1999). Wavelength dependence of the optical depth of biomass burning, urban, and desert dust aerosols. *J. Geophys. Res.* 104: 31333–31349.

Eck, T.F., Holben, B.N., Reid, J.S., Sinyuk, A., Dubovik, O., Smirnov, A., Giles, D., O'Neill, N.T., Tsay, S.C. and Ji, Q. (2008). Spatial and temporal variability of column - integrated aerosol optical properties in the southern Arabian Gulf and United Arab Emirates in summer. *J. Geophys. Res.* 113: D01204.

Giles, D.M., Holben, B.N., Eck, T.F., Sinyuk, A., Smirnov, A., Slutsker, I., Dickerson, R.R., Thompson, A.M. and Schafer, J.S. (2012). An analysis of AERONET aerosol absorption properties and classifications representative of aerosol source regions. *J. Geophys. Res.* 117: D17203.

Gobbi, G.P., Kaufman, Y.J., Koren, I. and Eck, T.F. (2007). Classification of aerosol properties derived from AERONET direct sun data. *Atmos. Chem. Phys.* 7: 453–458.

Higurashi, A. and Nakajima, T. (2002). Detection of aerosol types over the East China Sea near Japan from four-channel satellite data. *Geophys. Res. Lett.* 29: 1386.

Holben, B.N., Eck, T.F., Slutsker, I., Tanre, D., Buis, J.P., Setzer, A., Vermote, E., Reagan, J.A., Kaufman, Y.J., Nakajima, T., Lavenu, F., Jankowiak, I. and Smirnov, A. (1998). AERONET-A federated instrument network and data archive for aerosol characterization. *Remote Sens. Environ.* 66: 1–16.

Holben, B.N., Eck, T.F., Slutsker, I., Smirnov, A., Sinyuk, A., Schafer, J., Giles, D. and Dubovik, O. (2006). AERONET's Version 2.0 quality assurance criteria. Proc. SPIE 6408, Remote Sensing of the Atmosphere and Clouds, 64080Q.

Jeong, U., Kim, J., Lee, H., Jung, J., Kim, Y.J., Song, C.H. and Koo, J.H. (2011). Estimation of the contributions of long range transported aerosol in East Asia to carbonaceous aerosol and PM concentrations in Seoul, Korea using highly time resolved measurements: A PSCF model approach. *J. Environ. Monit.* 13: 1905–1918.

Jung, J., Kim, Y.J., Lee, K.Y., Cayetano, M.G., Batmunkh, T., Koo, J.H. and Kim, J. (2010). Spectral optical properties of long-range transport Asian dust and pollution aerosols over Northeast Asia in 2007 and 2008. *Atmos. Chem. Phys.* 10: 5391–5408.

Kaskaoutis, D.G. and Kambezidis, H.D. (2006). Investigation into the wavelength dependence of the aerosol optical depth in the Athens area. *Q. J. R. Meteorol. Soc.* 132: 2217–2234.

Kim, J., Lee, J., Lee, H.C., Higurashi, A., Takemura, T. and Song, C.H. (2007). Consistency of the aerosol type classification from satellite remote sensing during the Atmospheric Brown Cloud–East Asia Regional Experiment campaign. *J. Geophys. Res.* 112: D22S33.

Kim, J.Y., Kim, S.W., Ghim, Y.S., Song, C.H. and Yoon, S.C. (2012). Aerosol properties at gosan in Korea during two pollution episodes caused by contrasting weather conditions. *Asia-Pac. J. Atmos. Sci.* 48: 25–33.

Kolhe, A.R., Pawar, G.V., Varpe, S.R., Kumar, P.P., Devara, P.C.S. and Aher, G.R. (2016). Multi-year analysis of aerosol properties retrieved from the Ångström parameters for different spectral ranges over Pune. *Aerosol Air Qual. Res*. 16: 3266–3280.

Koo, J.H. (2008). *Optical properties of aerosol in a megacity, Seoul from ground-based and satellite measurements*. MS thesis, Yonsei University, Korea, 145 pp.

Koo, J.H., Kim, J., Lee, J., Eck, T.F., Lee, Y.G., Park, S.S., Kim, M., Jung, U., Yoon, J. and Mok, J. (2016). Wavelength dependence of Ångström exponent and single scattering albedo observed by skyradiometer in

Seoul, Korea. *Atmos. Res.* 181: 12–19.

Kumar, K.R., Sivakumar, V., Reddy, R.R., Gopal, K.R. and Adesina, A.J. (2014). Identification and classification of different aerosol types over a subtropical rural site in Mpumalanga, South Africa: Seasonal variations as retrieved from the AERONET Sunphotometer. *Aerosol Air Qual. Res.* 14: 108–123.

Lee, J., Kim, J., Song, C.H., Kim, S.B., Chun, Y., Sohn, B.J. and Holben, B.N. (2010). Characteristics of aerosol types from AERONET sunphotometer measurements. *Atmos. Environ.* 44: 3110–3117.

Lee, K., Park, J., Kang, M., Kim, D., Batmunkh, T., Bae, M.S. and Park, K. (2017). Chemical characteristics of aerosols in coastal and urban ambient atmospheres. *Aerosol Air Qual. Res*. 17: 908–919.

Li, J., Carlson, B.E. and Lacis, A.A. (2015). Using single-scattering albedo spectral curvature to characterize East Asian aerosol mixtures. *J. Geophys. Res.* 120: 2037–2052.

Mielonen, T., Arola, A., Komppula, M., Kukkonen, J., Koskinen, J., de Leeuw, G. and Lehtinen, K.E.J. (2009). Comparison of CALIOP level 2 aerosol subtypes to aerosol types derived from AERONET inversion data. *Geophys. Res. Lett.* 36: L18804.

Mishra, A.K. and Shibata, T. (2012). Synergistic analyses of optical and microphysical properties of agricultural crop residue burning aerosols over the Indo-Gangetic Basin (IGB). *Atmos. Environ.* 57: 205–218.

Mishra, A.K., Shibata, T. and Srivastava, A. (2014). Synergistic approach for the aerosol monitoring and identification of types over Indo-Gangetic Basin in pre-monsoon season. *Aerosol Air Qual. Res.* 14: 767–782.

Mok, J., Park, S.S., Lim, H., Kim, J., Edwards, D.P., Lee, J., Yoon, J., Lee, Y.G. and Koo, J.H. (2017). Correlation analysis between regional carbon monoxide and black carbon from satellite measurements. *Atmos. Res.* 196: 29–39.

O'Neill, N.T., Eck, T.F., Smirnov, A., Holben, B.N. and Thulasiraman, S. (2003). Spectral discrimination of coarse and fine mode optical depth. *J. Geophys. Res.* 108: 4559.

Ramanathan, V. and Carmichael, G. (2008). Global and regional climate changes due to black carbon. *Nat. Geosci.* 1: 221–227.

Reid, J.S., Eck, T.F., Christopher, S.A., Hobbs, P.V. and Holben, B. (1999). Use of the Ångstrom exponent to estimate the variability of optical and physical properties of aging smoke particles in Brazil. *J. Geophys. Res.* 104: 27473–27489.

Russell, P.B., Bergstrom, R.W., Shinozuka, Y., Clarke, A.D., DeCarlo, P.F., Jimenez, J.L., Livingston, J.M., Redemann, J., Dubovik, O. and Strawa, A. (2010). Absorption Angstrom Exponent in AERONET and related data as an indicator of aerosol composition. *Atmos. Chem. Phys.* 10: 1155–1169.

Sayer, A.M., Hsu, N.C., Eck, T.F., Smirnov, A. and Holben, B.N. (2014). AERONET-based models of smoke-dominated aerosol near source regions and transported over oceans, and implications for satellite retrievals of aerosol optical depth. *Atmos. Chem. Phys.* 14: 11493–11523.

Schuster, G.L., Dubovik, O. and Holben, B.N. (2006). Angstrom exponent and bimodal aerosol size distributions. *J. Geophys. Res.* 111: D07207.

Shang, X., Lee, M., Han, J., Kang, E., Kim, S.W., Gustafsson, Ö. and Chang, L. (2018). Identification and chemical characteristics of distinctive Chinese outflow plumes associated with enhanced submicron aerosols at the Gosan climate observatory. *Aerosol Air Qual. Res*. 18: 330–342.

Shindell, D. and Faluvegi, G. (2009). Climate response to regional radiative forcing during the twentieth century. *Nat. Geosci.* 2: 294–300.

Smirnov, A., Holben, B.N., Eck, T.F. and Slitsker, I. (2000). Clound-screening and quality control algorithms for the AERONET database. *Remote. Sens. Environ.* 73: 337–349.

Stein, A.F., Draxler, R.R., Rolph, G.D., Stunder, B.J.B., Cohen, M.D. and Ngan, F. (2015). NOAA's HYSPLIT atmospheric transport and dispersion modeling system. *Bull. Am. Meteorol. Soc.* 96: 2059–2077.

Torres, O., Ahn, C. and Chen, Z. (2013). Improvements to the OMI near-UV aerosol algorithm using A-train CALIOP and AIRS observations. *Atmos. Meas. Tech.* 6: 3257–3270.

Verma, S., Prakash, D., Ricaud, P., Payra, S., Attié, J.L. and Soni, M. (2015). A new classification of aerosol sources and types as measured over Jaipur, India. *Aerosol Air Qual. Res.* 15: 985–993.

Yoon, J., von Hoyningen-Huene, W., Kokhanovsky, A.A., Vountas, M. and Burrows, J.P. (2012). Trend analysis of aerosol optical thickness and Ångström exponent derived from the global AERONET spectral observations. *Atmos. Meas. Tech.* 5: 1271–1299.

Yu, J., Che, H., Chen, Q., Xia, X., Zhao, H., Wang, H., Wang, Y., Zhang, X. and Shi, G. (2015). Investigation of aerosol optical depth (AOD) and Ångström exponent over the desert region of Northwestern China based on measurements from the china aerosol remote sensing network (CARSNET). *Aerosol Air Qual. Res.* 15: 2024–2036.

Yuan, Y., Shuai, Y., Li, X.W., Liu, B. and Tan, H.P. (2014). Using a new aerosol relative optical thickness concept to identify aerosol particle species. *Atmos. Res.* 150: 1–11.

Received for review, December 3, 2017
Revised, April 11, 2018
Accepted, April 28, 2018